

Regulatory Insertion Removal Restores Maturation, Stability and Function of Δ F508 CFTR

Andrei A. Aleksandrov^{1,2}, Pradeep Kota^{3,4}, Luba A. Aleksandrov^{2,3}, Lihua He^{2,3}, Tim Jensen^{2,3}, Liying Cui^{2,3}, Martina Gentzsch^{2,5}, Nikolay V. Dokholyan^{3,4} and John R. Riordan^{2,3*}

¹Department of Biomedical Engineering, University of North Carolina-Chapel Hill, Chapel Hill, NC 27599, USA

²Cystic Fibrosis Treatment and Research Center, University of North Carolina-Chapel Hill, Chapel Hill, NC 27599, USA

³Department of Biochemistry and Biophysics, University of North Carolina-Chapel Hill, Chapel Hill, NC 27599, USA

⁴Molecular and Cellular Biophysics Program, University of North Carolina-Chapel Hill, Chapel Hill, NC 27599, USA

⁵Department of Cell and Development Biology, University of North Carolina-Chapel Hill, Chapel Hill, NC 27599, USA

Received 26 February 2010;

received in revised form

7 June 2010;

accepted 9 June 2010

Available online

16 June 2010

The cystic fibrosis transmembrane conductance regulator (CFTR) epithelial anion channel is a large multidomain membrane protein that matures inefficiently during biosynthesis. Its assembly is further perturbed by the deletion of F508 from the first nucleotide-binding domain (NBD1) responsible for most cystic fibrosis. The mutant polypeptide is recognized by cellular quality control systems and is proteolyzed. CFTR NBD1 contains a 32-residue segment termed the regulatory insertion (RI) not present in other ATP-binding cassette transporters. We report here that RI deletion enabled F508 CFTR to mature and traffic to the cell surface where it mediated regulated anion efflux and exhibited robust single chloride channel activity. Long-term pulse-chase experiments showed that the mature Δ RI/ Δ F508 had a $T_{1/2}$ of ~ 14 h in cells, similar to the wild type. RI deletion restored ATP occlusion by NBD1 of Δ F508 CFTR and had a strong thermostabilizing influence on the channel with gating up to at least 40 °C. None of these effects of RI removal were achieved by deletion of only portions of RI. Discrete molecular dynamics simulations of NBD1 indicated that RI might indirectly influence the interaction of NBD1 with the rest of the protein by attenuating the coupling of the F508-containing loop with the F1-like ATP-binding core subdomain so that RI removal overcame the perturbations caused by F508 deletion. Restriction of RI to a particular conformational state may ameliorate the impact of the disease-causing mutation.

© 2010 Elsevier Ltd. All rights reserved.

Edited by I. B. Holland

Keywords: ABC transporters; CFTR; cystic fibrosis; ion channel; DMD simulations

*Corresponding author. E-mail address: jack_rJordan@med.unc.edu.

Abbreviations used: CFTR, cystic fibrosis transmembrane conductance regulator; CF, cystic fibrosis; NBD1, N-terminal nucleotide-binding domain; CL, cytoplasmic loop; RI, regulatory insertion; ER, endoplasmic reticulum; SDR, structurally diverse region; DMD, discrete molecular dynamics; ABC, ATP-binding cassette; RMSF, root-mean-square fluctuations; MSD, C-terminal membrane-spanning domain; VRT-325, 4-cyclohexyloxy-2-[1-[4-(4-methoxy-benzensulfonyl)-piperazin-1-yl]-ethyl]-quinazolin; Corr-4a, *N*-[2-(5-chloro-2-methoxy-phenylamino)-4'-methyl-[4,5']bithiazolyl-2'-yl]-benzamide; PKA, protein kinase A; HEK, human embryonic kidney; BHK, baby hamster kidney; RIPA, radioimmunoprecipitation assay.

Introduction

The cystic fibrosis transmembrane conductance regulator (CFTR) is a hydrolyzable-ligand gated ion channel that employs the ATP-binding cassette (ABC) transporter structural architecture to couple ATP binding and hydrolysis with its anion channel activity.^{1,2} Although a very large number (~1600) of different mutations in the CFTR gene have been identified in patients with cystic fibrosis, a single mutation ($\Delta F508$) is present on at least one allele in 90% of patients†. The deletion of the F508 residue from the N-terminal nucleotide-binding domain (NBD1) of CFTR prevents normal folding and assembly of the protein so that it is recognized as abnormal by quality control systems and cleared from both the early and the late secretory pathways. However, under certain conditions where the mutant molecule is able to avoid this fate, it is at least partially functional as an anion channel at the cell surface.³ These conditions include maintenance of cells expressing the protein at low temperature⁴ and exposure to osmolytes⁵ or certain small molecules either binding to the protein or acting on the cellular quality control apparatus.^{6,7} There are also a number of second-site amino acid substitutions that partially restore conformational maturation, intracellular trafficking and function of $\Delta F508$ CFTR.^{8–10} Thus, development of means to overcome or circumvent the effect of the F508 deletion would provide an important therapeutic strategy for treatment of the disease. Increased understanding of the nature of the disruption of the molecule caused by the absence of F508 is necessary for the implementation of such strategies. For example, the finding that the absence of F508 from the surface of NBD1 perturbs its interaction with a cytoplasmic loop (CL4) in the C-terminal membrane-spanning domain (MSD2) has focused attention on this interface between domains as a target of stabilizing small molecules.¹¹

While the overall three-dimensional structure of the isolated NBD1, as determined by X-ray crystallography, is not altered by the $\Delta F508$ mutation,¹² both the folding yield¹³ and the pathways¹⁴ of the domain are different from those of the wild type. A unique feature of CFTR NBD1 relative to the NBDs of all other ABC proteins is the insertion of a 32-residue segment between the first two beta strands in the structure of the domain.¹⁵ The role of this extra polypeptide, which has been termed the regulatory insertion (RI), in CFTR structure and function is unknown, as deletion of most of it including the protein kinase A (PKA) phosphorylation site at serine 422 apparently has little effect on the expression and channel function of wild-type CFTR in *Xenopus* oocytes.¹⁶ However, very recently it was shown that complete RI deletion promotes homodimer formation and stability of NBD1 with only minor structural changes upon F508 deletion.¹⁷

We hypothesized that the absence of the RI might improve the stability of full-length $\Delta F508$ CFTR expressed in mammalian cells. We found that unlike the influence of many mutations in NBD1, deletion of the complete RI sequence did not impair expression and processing of wild-type CFTR but on the contrary promoted the maturation of $\Delta F508$ CFTR. Not only did the RI-deleted $\Delta F508$ CFTR escape endoplasmic reticulum (ER) quality control and reach the Golgi apparatus to acquire complex oligosaccharide chains, but it also was stabilized at the cell surface where it mediated robust chloride channel activity. Discrete molecular dynamics simulations showed that coupling between the dynamics of the F508-containing loop and the F1-like ATP-binding core subdomain of NBD1 disappeared upon F508 deletion. Furthermore, there was a dramatic increase in the flexibility of the structurally diverse region (SDR) involved in contacts of NBD1 with the first cytoplasmic loop (CL3) in the C-terminal MSD. Both changes were at least partially overcome by RI deletion. Overall, our findings reveal that the presence of the functionally nonessential RI is a major contributor to the structural and functional instability of $\Delta F508$ CFTR.

Results

RI deletion enables $\Delta F508$ CFTR maturation and traffic to the cell surface

The structure and position of RI as seen in the X-ray structure of mouse NBD1 is shown in Fig. 1 with alpha helical elements at both ends and a very short helix containing the serine 422 PKA phosphorylation site in the middle. Although the deletion of the last two-thirds of the segment has been found to

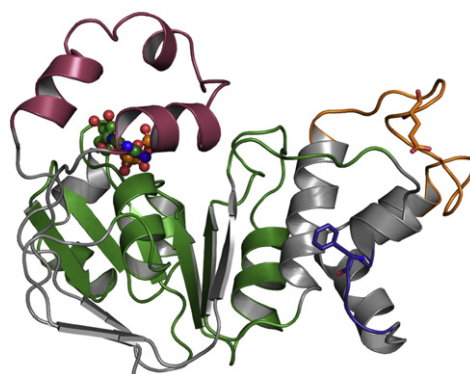


Fig. 1. Structural features of wild-type CFTR-NBD1. The structure of CFTR NBD1 (PDB code 2BBO) is shown. F1-like ATP-binding core subdomain (G451–L475, D565–Q637) and γ -switch (Q493–P499) are in green. The RI region of NBD1 is colored red. ATP is shown in ball-and-stick representation. The 507–511 loop is colored blue and the side chain of F508 is shown in ball-and-stick representation. The 536–550 SDR loop is colored orange. Loops are rendered thicker than normal for easier visualization.

† <http://www.genet.sickkids.on.ca/cftr/app>

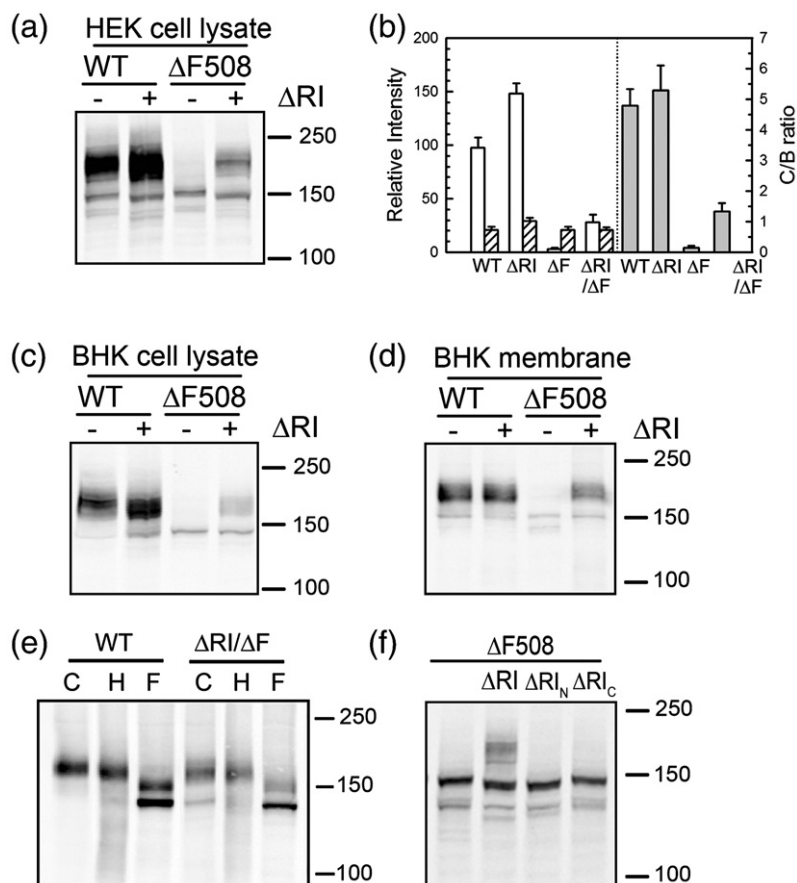


Fig. 2. Deletion of RI promotes maturation of $\Delta F508$ CFTR. (a) Cell lysates containing 50 μ g of total protein from transiently transfected HEK 293 cells were subjected to Western blot analysis using anti-CFTR antibody mAb596. (b) The relative intensities of both mature and immature bands normalized to the wild-type CFTR mature band and ratio of mature to immature band intensities are shown. The open and hatched bars represent mature and immature bands, respectively. The gray bars on the right represent the ratio of mature to immature band intensities. All data are shown as mean \pm SEM from three independent experiments. Western blots (mAb596) of cell lysates with 50 μ g of total protein are shown in (c) and membranes with 10 μ g of total protein in (d) from BHK cells stably expressing CFTR variants. (e) Membrane vesicles prepared from BHK cells expressing WT and $\Delta RI/\Delta F508$ -CFTR were treated with endoglycosidase H or N-glycanase F before subjecting to Western blot analysis. Note that N-glycanase digestion results in two bands of higher mobility, the smaller representing

the completely deglycosylated protein from which both N-linked chains have been removed and the larger intermediate band, the product with only the more susceptible chain removed. C, control; H, endoglycosidase H; F, N-glycanase F. (f) Western blots (mAb596) of HEK 293 cells transiently transfected with $\Delta F508$ -CFTR with the entire RI (ΔRI), N-terminal portion (ΔRI_N) or C-terminal portion (ΔRI_C) deleted. ΔRI_N and ΔRI_C refers to the deletion of RI fragments 404–412 and 414–432, respectively.

have little effect on channel activity in *Xenopus* oocytes,¹⁶ we postulated that the presence or the absence of the entire large-peptide insertion might have some influence on the assembly and stability of the molecule. Because the $\Delta F508$ mutation strongly influences both of these parameters, we tested the effect of RI removal on the behavior of $\Delta F508$ CFTR in mammalian cells. Strikingly, the complete RI deletion resulted in very substantial maturation of $\Delta F508$ CFTR when expressed transiently in human embryonic kidney (HEK) 293 cells or stably in baby hamster kidney (BHK) cells as evidenced by appearance of the more slowly migrating band in Western blots (Fig. 2). Quantification of the band intensities indicated that the steady-state amount of the $\Delta RI/\Delta F508$ more slowly migrating mature form was approximately one-third that of the wild type in the 293 cells (Fig. 2b). Maturation of $\Delta RI/\Delta F508$ CFTR also occurred in other cell types including BHK cells (Fig. 2c) and was enriched in their isolated membranes (Fig. 2d). That the mature band contained complex N-linked oligosaccharide chains added in the Golgi apparatus is shown by its sensitivity to N-glycanase but not to endoglycosidase-H (Fig. 2e). Thus, while the degree of maturation of $\Delta F508$ is still considerably less than that of

the wild type, it is comparable to or exceeds that resulting from other means of rescue including growth of cells at low temperature, suppressor or solubilizing single-residue substitutions in NBD1 or small corrector molecules.^{7,18} Estimation of the amount of $\Delta RI/\Delta F508$ CFTR that reaches the cell surface is described below. The maturation of $\Delta F508$ CFTR was achieved only by deletion of the entire RI fragment, as deletion of just the N-terminal or C-terminal portion did not have this effect (Fig. 2f). Although we have not studied the influence of RI deletion on wild-type CFTR in detail, its maturation also was augmented as clearly indicated in Fig. S1.

To determine whether removal of RI had stabilized $\Delta F508$ CFTR in terms of its lifetime in the cell, long-term pulse-chase experiments were performed. As seen in Fig. 3a, mature $\Delta RI/\Delta F508$ decayed at a rate similar to that of wild-type CFTR, indicating that there had been substantial stabilization of the mutant protein, which, when unmodified, decays very rapidly.²¹ As might be expected from the amount of mature $\Delta RI/\Delta F508$ protein, much of it is localized to the cell surface, as can be seen by immunofluorescence staining (Fig. 3b, left upper panels). The plasma membrane pool is particularly well delineated after cells have been treated with cycloheximide so that

the intracellular pool of immature protein is depleted (Fig. 3b, left lower panels). Under these conditions, it was possible to quantify the intensity of the cell surface fluorescence due to immunostaining of $\Delta RI/\Delta F508$ relative to wild-type CFTR (Fig. 3b, right panel). By these estimates, the density of the restored mutant protein on the cell surface was approximately 60% of that of the wild type. This proportion is larger than that of the mature protein bands in the two cell types in Western blots (Fig. 2), possibly suggesting that the surface pool may be stabilized more than the total post-ER pool with complex oligosaccharide chains. Alternatively, the difference between the $\sim 30\%$ and $\sim 60\%$ estimates may largely reflect differences between the two methods.

There is little or no $\Delta F508$ CFTR protein at the surface of stably expressing BHK cells grown at 37°C . Accordingly, there is a barely detectible cyclic AMP-stimulated iodide efflux response by these cells (Fig. 3c, left panel). However, with cells

expressing $\Delta F508$ CFTR from which the RI has been deleted, efflux is strongly stimulated when cellular cyclic AMP is increased (Fig. 3c, dotted line). While the response is significantly delayed compared to that of cells expressing wild-type CFTR, the overall magnitude is similar. This result provides evidence that the $\Delta RI/\Delta F508$ protein that is able to traffic to the cell surface is functional. In addition, when the relative single-channel properties of $\Delta RI/\Delta F508$ and wild-type CFTR are taken into account (see Figs. 7 and 8), the cumulative efflux data (Fig. 3c, right panel) also provide an estimate of the relative amounts of active protein in the plasma membrane. Because the slopes of those efflux curves differ by a factor of 4, while the open probability of $\Delta RI/\Delta F508$ at 25°C is approximately one-half that of the wild type, the number of rescued mutant CFTR channels should be approximately half of the wild type, in general agreement with the estimates by the other two methods.

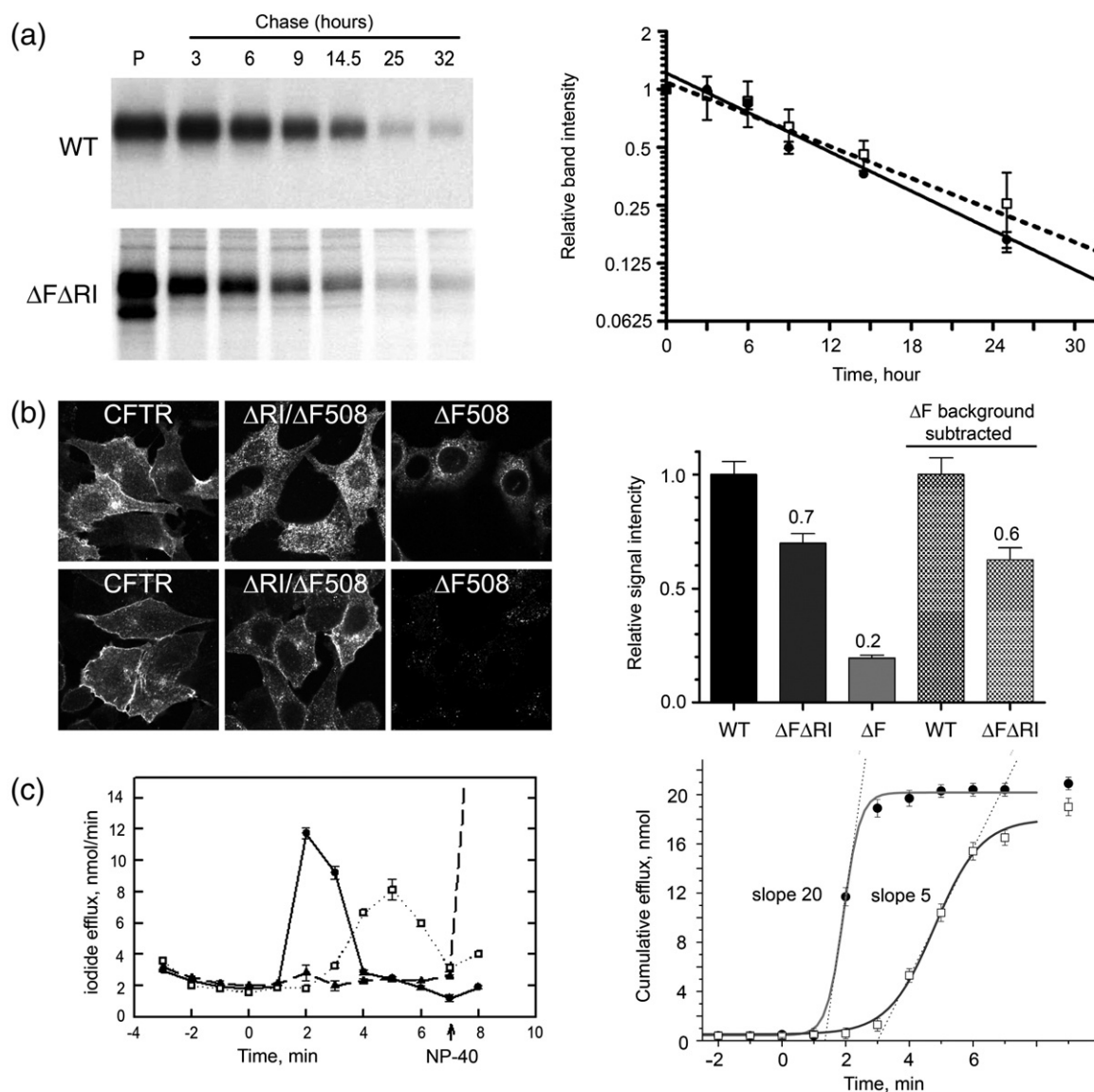


Fig. 3 (legend on next page)

RI deletion restores the ability of $\Delta F508$ CFTR to bind and trap ATP at NBD1

The first ATP-binding site in CFTR occludes but does not hydrolyze ATP, whereas the second site is hydrolytic.^{22,23} This behavior is reflected by the fact that $8N_3$ ATP is stably bound to NBD1 prior to its covalent attachment by photoactivation, whereas the nucleotide bound to NBD2 may rapidly dissociate. $8N_3[\gamma\text{-}^{32}\text{P}]\text{ATP}$ bound to defined NBD containing fragments produced by limited proteolytic digestion is readily detected and quantified by autoradiography after SDS-PAGE. Thus, after incubation of CFTR containing membranes with $8N_3[\gamma\text{-}^{32}\text{P}]\text{ATP}$, the products of hydrolysis are readily washed away from NBD2, while the unhydrolyzed nucleotide is retained at NBD1 [Fig. 4a, wild type (WT)]. Although at 4 °C there is weak nucleotide binding to NBD1 of temperature-rescued $\Delta F508$ CFTR, this binding does not withstand washing, indicating that it is not trapped as in the wild type (Fig. 4a, $\Delta F508$). In $\Delta RI/\Delta F508$ CFTR the trapping of the nucleotide is restored, making it resistant to washing from NBD1. The detection of the bound nucleotide in a larger NBD1 containing tryptic fragment (~70 kDa) when RI is deleted, compared with a fragment of ~40 kDa when it is present, is due to the removal of a trypsin cleavage site within the RI.²⁴ This difference is also evident in the RI-deleted wild type (Fig. 4a, ΔRI). The data in Fig. 4a clearly show that the ability of wild-type NBD1 to stably trap the nucleotide, which is lost in $\Delta F508$, is reestablished by deletion of RI.

The weak nucleotide binding to NBD1 of temperature-rescued $\Delta F508$ CFTR completely disappeared when the temperature of the CFTR containing membranes was increased from 4 to 35 °C (Fig. 4b, right two lanes). More importantly, when RI was deleted, the ability of $\Delta F508$ CFTR to retain the nucleotide at 35 °C was completely restored (Fig. 4b, middle two lanes), as in the wild-type CFTR (Fig. 4b, left two lanes). These results substantiate those in Fig. 4a and emphasize the capacity of RI removal to compensate for the effect of the $\Delta F508$ mutation on the ability of NBD1 to trap ATP.

Further evidence of the restored ability of $\Delta RI/\Delta F508$ to retain ATP bound at NBD1 is shown in Fig. 4c and d, where the slow rate of dissociation at 35 °C is very similar to that of the wild type with a $T_{1/2} > 30$ min.²⁵ Thus, in addition to extending the lifetime of $\Delta F508$ CFTR protein to the same range as that of the wild type, RI deletion also restored the capacity of $\Delta F508$ NBD1 to bind and occlude ATP to a very similar extent as wild type.

RI deletion restores cross-linking of domain interfaces in $\Delta F508$ CFTR

The $\Delta F508$ mutation disrupts interdomain contacts in CFTR including those so-called domain-swapping interactions between sites on either NBD and CLs in MSDs on the opposite side of the molecule.^{11,26} To determine if these interfacial contacts are restored on deletion of RI, pairs of cysteine residues were introduced at these locations in Cys-less $\Delta F508$ CFTR constructs in which RI was

Fig. 3. Deletion of RI promotes maturation, lifetime on the cell surface and function of $\Delta F508$ CFTR. (a) WT and $\Delta RI/\Delta F508$ CFTR cells were pulsed with [^{35}S]methionine for 8 h and the disappearance of the mature protein was followed during a 32-h chase. Quantification of the bands and single-exponential fit for both the wild-type and the $\Delta RI/\Delta F508$ CFTR in the graph to the right show that the two have similar turnover kinetics with a $T_{1/2}$ of ~12 h for WT (filled circle, continuous line) and ~14 h for the mutant (open square, dashed line). Each experimental point is shown as a mean \pm SEM from three independent experiments. (b) Immunofluorescence microscopy of BHK cells stably expressing WT, $\Delta RI/\Delta F508$ and $\Delta F508$ CFTR was performed on fixed and permeabilized cells using anti-CFTR mouse monoclonal antibody 570, followed by goat anti-mouse IgG Alexa Fluor 488 conjugate (upper row). Cells also were treated with 100 μM cycloheximide for 4 h before immunostaining to deplete the intracellular pool of immature protein (bottom row). The cycloheximide-treated cells were used to estimate surface density of CFTR variants by quantifying the fluorescence intensity. Using ImageJ, a 250×250 -pixel square was defined and the average pixel intensity within was measured. Then the region was moved to cover several cells per image and several images were measured per each variant (WT, $n=61$; $\Delta RI/\Delta F508$, $n=74$; $\Delta F508$, $n=41$). The background was measured from several cell-free areas of the individual images and subtracted from the cell measurements to correct for variations in image brightness between images. Measurements were normalized to the WT average value and shown on the graph at the right (three bars from the left). Because a 3-h cycloheximide treatment can clear $\Delta F508$ CFTR signal from a Western blot,^{19,20} our 4-h treatment should have been sufficient. The residual signal seen in the $\Delta F508$ CFTR images probably represents degradation products that are still detectable. The two bars on the right represent relative intensities when $\Delta F508$ CFTR background is subtracted. (c) CFTR channel activity measured by iodide efflux assay using BHK cells expressing WT CFTR (filled circles, continuous line), $\Delta RI/\Delta F508$ CFTR (open square, dotted line) or $\Delta F508$ CFTR (filled triangle, dashed line). Cells were loaded with iodide and efflux was measured using an iodide-selective electrode. The stimulation cocktail was added at time 0 to activate efflux through CFTR channels. The values represent the mean \pm SEM of the amount of iodide released from the cells during each 1-min interval ($n=3$). At the end of each assay, efflux buffer containing 0.1% NP-40 was added (arrow) to release retained iodide. These efflux data were transformed to yield the cumulative iodide efflux graph on the right. This provides a numerical estimation of cellular membrane permeabilities. The maximum slope of the tangent line to the best fit of the data set is a reasonable estimation of the maximum value of efflux $J \sim NP_o$. The ratio of maximum slopes ($J_{\Delta RI/\Delta F508}/J_{wt} \approx (NP_o)_{\Delta RI/\Delta F508}/(NP_o)_{wt} \approx 5/20 = 0.25$). If the ratio of $(P_o)_{\Delta RI/\Delta F508}/(P_o)_{wt}$ is about 0.5 (Figs. 7a and 8a), then $N_{\Delta RI/\Delta F508}/N_{wt} = 0.5$ is an upper estimate. Nearly identical values of the total efflux for the WT and $\Delta RI/\Delta F508$ CFTR after cell solubilization by NP-40 (indicated by symbols separated from the curves) provide evidence of similar iodide loading of similar numbers of cells.

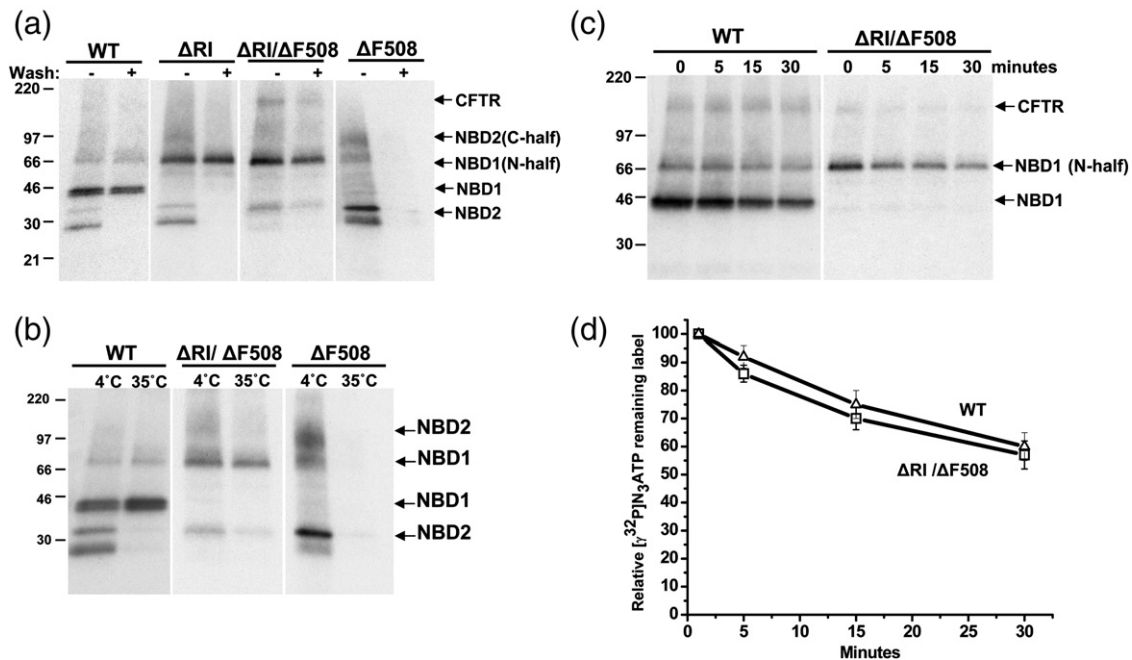


Fig. 4. ATP binding and occlusion by $\Delta F508$ CFTR at 35 °C is restored upon RI deletion. (a) Membranes from BHK cells expressing WT or mutant CFTR after $8N_3[\gamma-^{32}P]ATP$ binding at 4 °C were UV-irradiated before or after washing away free radioactive nucleotide, as indicated. After limited trypsin digestion and solubilization in RIPA buffer, the tryptic fragments were immunoprecipitated with monoclonal antibodies 13-4 and 596, resolved by SDS-PAGE (4–20% acrylamide) and subjected to autoradiography. (b) Membrane proteins after incubation with $8N_3[\gamma-^{32}P]ATP$ at 4 °C or 35 °C for 5 min were UV-irradiated and treated as in (a). (c) Membranes from cells expressing wild-type and mutant CFTR were incubated with $8N_3[\gamma-^{32}P]ATP$ and free nucleotide was washed away. The membrane pellets were resuspended in nucleotide-free buffer and samples were UV-irradiated after incubation at 35 °C for the indicated periods. The photolabeled proteins were digested and analyzed as in (a) but using only mAb 13-4. (d) Quantification of autoradiogram from (c) by electronic radiography.

either present or absent (Fig. 5). Treatment of cells expressing these constructs with bifunctional methanethiosulfonate reagents resulted in cross-linking of members of both these cysteine pairs when RI had been removed, indicating reestablishment of native-like contacts between NBD2 and CL2 as well as NBD1 and CL4. Thus, RI removal from $\Delta F508$ NBD1 brings about the restoration of disrupted interactions between domains throughout the molecule.

RI deletion restores stable $\Delta F508$ CFTR channel activity

The cAMP-stimulated iodide efflux from $\Delta RI/\Delta F508$ CFTR-expressing cells (Fig. 3c) indicated its functional capability. However, single-channel gating provides the most sensitive measure of CFTR function. When $\Delta F508$ CFTR molecules reach the surface of cells grown at reduced temperature or treated with osmolytes or so-called corrector small molecules, attenuated channel activity is observed.^{27–30} When assayed at room temperature, this activity persists, at least during the periods of the assays, but is lost very rapidly at physiological temperature.^{29,31,32} This behavior is detailed in Fig. 6 for channels in membranes of $\Delta F508$ CFTR-expressing cells grown at 27 °C and treated with correctors VRT-325 [4-cyclohexyloxy-

2-[1-[4-(4-methoxy-benzensulfonyl)-piperazin-1-yl]-ethyl]-quinazolin] and Corr-4a [N-[2-(5-chloro-2-methoxy-phenylamino)-4'-methyl-[4,5'] bithiazolyl-2'-yl]-benzamide] in combination (see Fig. 9). The heterogeneous nature of the gating kinetics is immediately apparent from visual inspection of 10 min of recording at +25 °C (Fig. 6a). The reversible interconversion between patterns of activity with two different conductances is confirmed by two well-defined peaks (10.6 ± 0.4 and 6.1 ± 0.6 pS) for the open states in the all-points histogram shown on the left. The fact that both conductive states belong to the same functional unit is confirmed by the absence of their superposition in these records with hundreds of transitions between open and closed states as well as direct gradual interconversion between distinct open states (not shown). The latter are very rare events, and in most cases, interconversion proceeds in the closed state. The patterns of activity persist long enough to be easily separated for further analysis. However, the problem of $\Delta F508$ CFTR nonstationary gating kinetics for the patterns with fully open state precludes kinetic analysis with a high degree of confidence.²⁹ At least three different patterns of activity do occur at +25 °C, as shown in Fig. 6b–d. The patterns of activities shown in Fig. 6b and c have conductance of 10.6 pS and P_o values progressively decreasing in time from the nearly wild-type value of 0.26 at the beginning to the low 0.04 value between 6

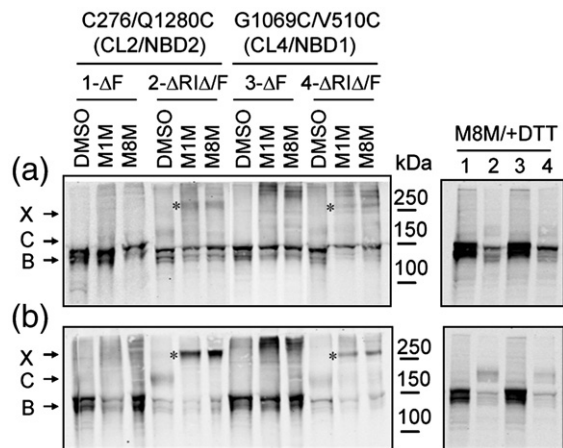


Fig. 5. Restoration of MSD–NBD interfaces by RI deletion from $\Delta F508$ CFTR. HEK 293 cells were transiently transfected with Cys-less $\Delta F508$ CFTR with Cys pairs introduced at the CL2–NBD2 (C276–Q1280C) or CL4–NBD1 (V510C–G1069C) interfaces in the absence or presence of ΔRI . Twenty-four hours after transfection, cells were grown for a further 24 h at 37 °C (a) or 27 °C (b). Cells were harvested and washed, and cross-linking of Cys pairs with 200 μ M of MTS cross-linkers (M1M and M8M) was carried out as described before.¹¹ Cell lysates in SDS-PAGE sample buffer with or without DTT as indicated were subjected to Western blot analysis using mAb596. X, cross-linked CFTR (bands also marked by asterisks); C, mature complex-glycosylated CFTR; B, immature core-glycosylated CFTR.

and 8 min of recording for the experiment shown in Fig. 6a. In different experiments, the overall P_o for the full open-state conductance may vary from 0.26 to 0.04. Only the activity shown in Fig. 6d with a stable subconductance level of 6.1 pS and $P_o = 0.52$ remains after 15 min at +25 °C.

The single-channel activity exhibited at +35 °C is shown in Fig. 6e where the only peak in the all-points histogram is that of the stable closed state. No stable open states occur at this temperature, but some unresolved brief openings could result in a leak current in whole-cell recordings. Further progressive loss of activity occurs as temperature is ramped from +35 to +40 °C (Fig. 6f) with the closed state predominant at +40 °C where only very rare and brief unresolved openings are visible (Fig. 6g).

Examination of the single-channel properties of $\Delta RI/\Delta F508$ CFTR using the same experimental protocols showed very different results (Fig. 7). First unlike the unmodified $\Delta F508$, stable activity was observed at 25 °C with homogeneous full-conductance openings (Fig. 7a). The open probability of 0.12 was approximately half that of the wild type under the same conditions (see Fig. 8a). Recording at 35 °C, where virtually no stable openings of $\Delta F508$ channels could be detected, revealed uniform gating transitions having an open probability only ~20% less than that of the wild type and with identical conductance (compare Figs. 7b and 8b). Most strikingly, during continuous tem-

perature increase from 35 to 40 °C, gating persisted and accelerated with the expected increase in conductance (Fig. 7c). This behavior mimicked that of the wild type (Fig. 8c), as did the persistent stable gating when the channels were held at 40 °C for prolonged periods (compare Figs. 7a and 8a). These data emphasize that the major impact of the removal of the complete RI from $\Delta F508$ CFTR is to overcome the functional failure of the channel in the physiological temperature range caused by F508 deletion.

RI deletion increases the sensitivity of $\Delta F508$ to small-molecule correctors

To investigate the relationship of RI deletion to other manipulations that promote maturation of $\Delta F508$, we tested the effects of both the growth of cells at reduced temperature and exposure to small-molecule corrector compounds.^{7,33} As seen in Fig. 9, a small amount of mature band C appeared in cells expressing $\Delta F508$ CFTR grown at 27 °C (lane 5), and this was greatly increased on simultaneous exposure to the two corrector compounds Corr-4a and VRT-325 (lane 6). However, at 37 °C, there was only a very modest response to the two compounds (compare lanes 11 and 12). This is consistent with the general experience that these compounds are much more effective at lower than at higher temperature. With the RI-deleted $\Delta F508$, however, the effects of low temperature and these corrector compounds separately or together appeared to be quite different. First, the degree of maturation of $\Delta RI/\Delta F508$ (amount of band C) was fairly similar at 27 °C (lane 1) and 37 °C (lane 7), indicating that when the RI is not present the temperature sensitivity of the $\Delta F508$ mutant is reduced. Second, compound VRT-325 alone caused a similar further increase in maturation of $\Delta RI/\Delta F508$ at both temperatures (lanes 2 and 8). While of lesser magnitude, the stimulation caused by Corr-4a also was not greatly different at the two temperatures (lanes 3 and 9). More striking was the influence of the two compounds acting together where the extent of maturation was as great at 37 °C (lane 10) as at 27 °C (lane 4) and in the same range as the wild type. As already noted, this degree of correction of $\Delta F508$ containing the RI by the two compounds is only possible at the lower temperature (lane 6). Thus, these observations are consistent with the idea that the presence of the RI contributes substantially to the thermosensitivity of the $\Delta F508$ polypeptide. The fact that the effects of RI removal and at least these two correctors are distinct and additive, whereas there is some commonality to the effects of RI deletion and low temperature, suggests that these compounds do not act at the level of the RI and is consistent with RI influencing the thermodynamic stability of the protein.

Influence of RI on NBD1 dynamics

The rescue of $\Delta F508$ by the deletion of the RI region suggests a potential dynamic coupling

between the RI region and the F508-containing segment. Mutations in other sites in NBD1, such as the I539,¹⁰ F494/Q637, and F429/F494/Q637,⁸ partially attenuate the trafficking and gating defect of the full-length $\Delta F508$ CFTR. The mechanism by

which RI deletion and single-residue substitutions within NBD1 rescue $\Delta F508$ is unknown. However, these observed compensatory effects suggest the plausible hypothesis that these regions may be dynamically coupled. To investigate this possibility,

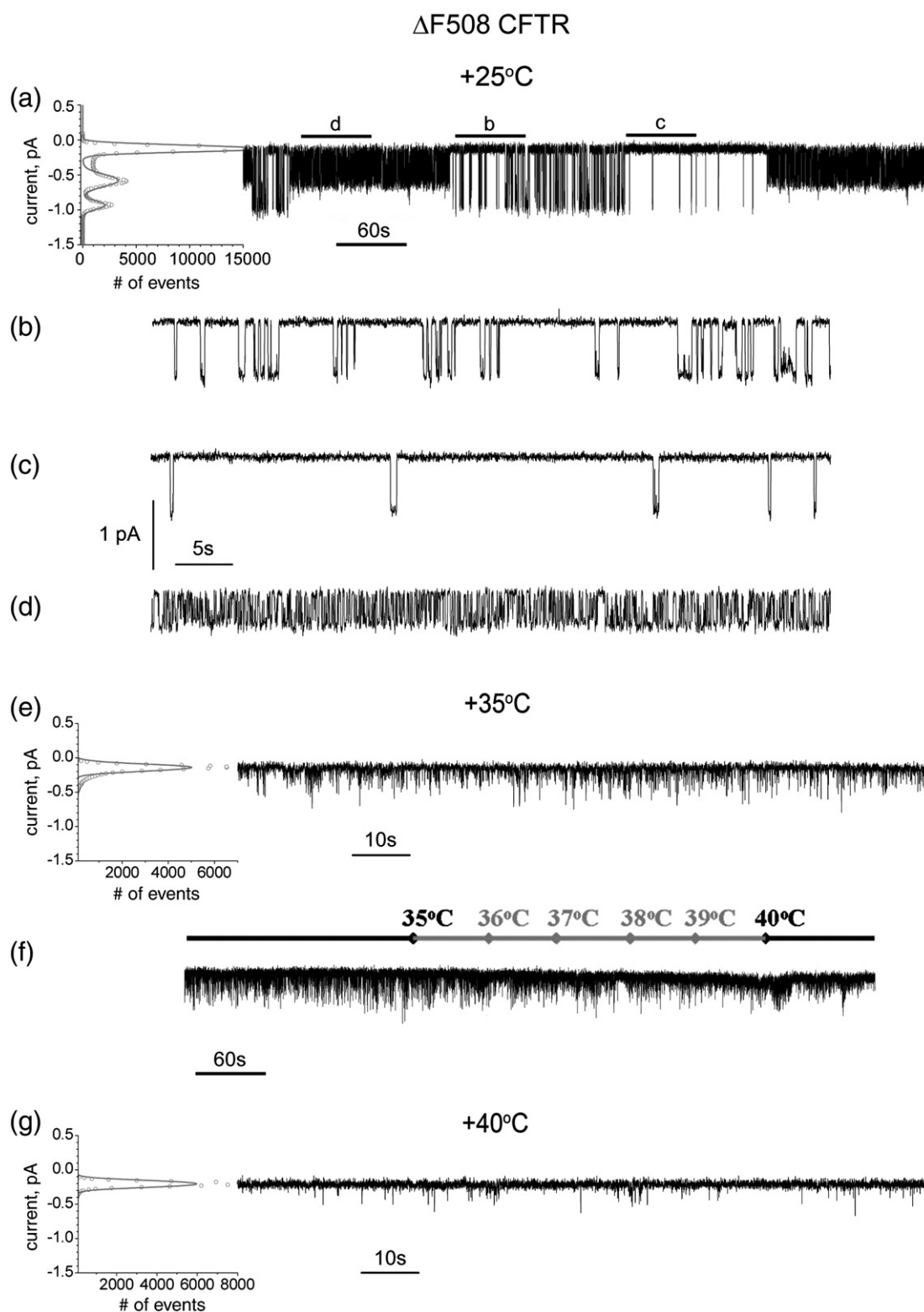


Fig. 6 (legend on next page)

we performed discrete molecular dynamics (DMD) simulations^{34,35} of both wild-type and $\Delta F508$ NBD1 with and without the RI. In order to determine the conformational flexibility of NBD1, we computed the root-mean-square fluctuations (RMSF) for each amino acid in NBD1 for all the NBD1 constructs during the course of a simulation (Fig. 10a). We find that the RI region is indeed flexible and dynamic, which is in agreement with the observed elevated *B*-factors in the NBD1 crystal structures¹⁵ and NMR studies.³⁶ This flexibility of RI in wild-type CFTR NBD1 is comparable to that in $\Delta F508$ CFTR NBD1. However, the SDR (L526–T547) of the domain containing residue I539, one of the sites targeted for rescue of the $\Delta F508$ defect,¹⁰ shows increased flexibility in the $\Delta F508$ background, compared to WT CFTR NBD1 with maximum difference in the RMSF values at residue E543. After RI deletion, the flexibility of this region is restored to the wild-type level. In view of these results, we propose that the flexibility of the RI region is dynamically coupled to the SDR region, suggesting that deletion of the RI region is equivalent to incorporating restorative mutations at this and other sites.

To further evaluate the probable dynamic coupling of distant sites in CFTR-NBD1, we performed covariance analysis (see Materials and Methods) on the entire domain (Fig. 10b). In our analyses, if two sites in NBD1 move in concert, even if sequentially and spatially distant from each other, the sites are considered to be correlated. We observed that the dynamics of the F508-containing loop is coupled to that of the SDR (Fig. 10b), both of which have been hypothesized to participate in formation of the interface with CL3 and CL4 in MSD2,^{11,26} and this coupling was not strongly affected by F508 deletion. We constructed normalized correlation maps for NBD1 from the simulation trajectories to estimate coupling between different regions of NBD1. Each correlation map is an $N \times N$ covariance matrix (where N is the length of the protein) of correlation coefficients derived from the simulation trajectory. The covariance matrix describes the correlation of the positional fluctuations of α carbon atoms of different residues in NBD1. The correlation coefficient ranges from -1 to 1 , where a value of 1 represents strong positive correlation (red dots in Fig. 10b), while a value of -1 denotes strong negative correlation (blue dots in Fig. 10b). We find that the dynamics of the loop containing F508 and the RI region are not coupled in the wild-type

NBD1 (yellow region in Fig. 10b). However, the F508-containing loop demonstrates strong correlations in dynamics with the F1-like ATP-binding core subdomain (blue dots in Fig. 10b). These correlations were completely lost upon F508 deletion and were at least partially restored upon removal of the RI region (Fig. 10b). This observation suggests the possibility that the RI region may regulate the coupling of movements of the F508-containing segment with the F1-like ATP-binding core subdomain of NBD1. In light of the fact that the structure of NBD1 is not significantly different with and without F508,³⁷ we hypothesize that it is not the structure but the dynamics of NBD1 that has the greater influence on CFTR trafficking, maturation and function.

Discussion

The way in which the absence of a single residue (F508) compromises the CFTR molecule in most patients with cystic fibrosis has remained incompletely understood. The end result of the mutation is that, although fully synthesized at a normal rate, most of the nascent polypeptide is ubiquitinated and succumbs to proteasomal degradation at the ER.^{39,40} Much has been learned about how the quality control apparatus appraises and culls the aberrantly assembled molecules both co- and posttranslationally.^{19,41} Manipulation of different components of this apparatus including multiple molecular chaperones has been attempted as a means of improving the maturation of $\Delta F508$ CFTR. In one case, down-regulation of the Hsp90 co-chaperone, Aha-1, had at least a partial positive effect,⁴² and efforts of this type are continuing. Some of the small molecules turned up in cell-based high-throughput screens probably act on constituents of the biosynthetic processing and quality control systems, as they are not entirely specific for CFTR. Other so-called correctors may bind directly to CFTR, but as yet there is limited evidence supporting this hypothesis.⁴³ Understanding of the mechanism of action of this latter group of small molecules and the development of improved ones is impaired by the fact that the exact influence of the lack of F508 on the CFTR protein is still unclear. While it has become apparent that the absence of the residue from the surface of NBD1 precludes its normal interaction with the last CL in the C-terminal

Fig. 6. Single-channel recordings of $\Delta F508$ CFTR at different temperatures. (a) Ten-minute recording of a temperature- and corrector-rescued $\Delta F508$ CFTR single channel at $+25^\circ\text{C}$. The reversible interconversion between patterns of activity with two different conductances of 10.6 ± 0.4 and 6.1 ± 0.6 pS was confirmed by two well-resolved peaks of open states in the all-points histogram shown on the left. The peak values were found from multiple peak Gaussian fitting and used to calculate conductance and standard deviation. The different patterns of activities in (a) are displayed in extended time scale in (b), (c) and (d). The locations of these patterns in the entire recording in (a) are marked by continuous lines above. (d) Only an activity with a stable conductance level of 6.1 pS and $P_o = 0.52$ was detected after 15 min incubation in the experimental chamber at $+25^\circ\text{C}$. (e) At $+35^\circ\text{C}$ no stable open states were detected, while unresolved brief openings still occur and are large in number. (f) Further loss of functional ability occurred when the temperature was continuously increased from $+35^\circ\text{C}$ to $+40^\circ\text{C}$ at a rate of $1^\circ\text{C}/\text{min}$. (g) Residual channel activity with very rare and brief openings was observed at $+40^\circ\text{C}$.

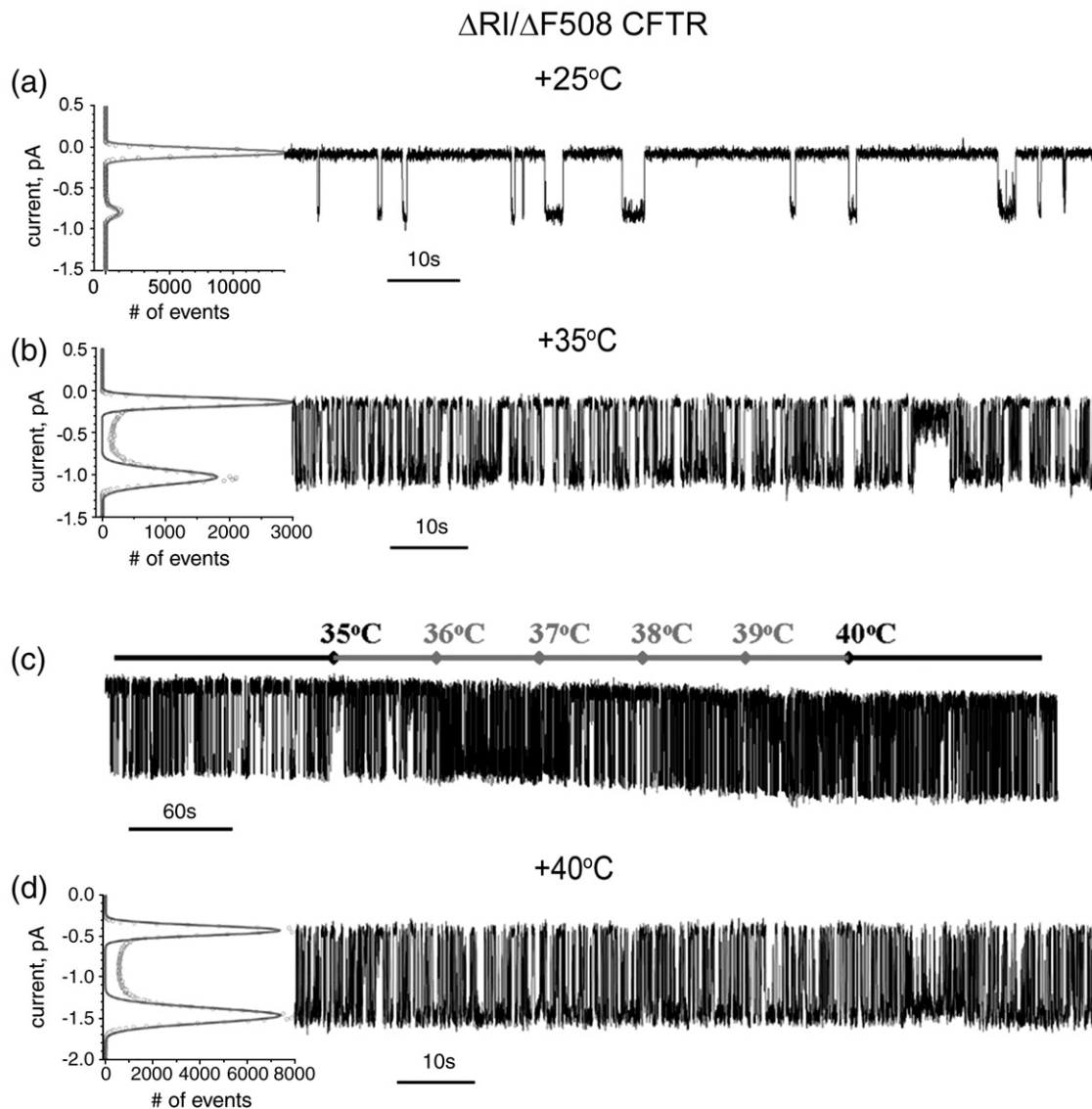


Fig. 7. RI deletion stabilizes $\Delta F508$ CFTR channel activity. (a) Two-minute recording of a $\Delta RI/\Delta F508$ CFTR single channel at +25 °C is shown at the right. All-points histogram used to calculate P_o and γ is shown at the left. Unlike rescued $\Delta F508$ CFTR, $\Delta RI/\Delta F508$ CFTR has stable activity at +25 °C with $P_o = 0.12 \pm 0.03$ and $\gamma = 10.6 \pm 0.3$ pS calculated from six independent experiments of 54 min total duration. (b) All-points histogram used to calculate single-channel parameters and 2 min of $\Delta RI/\Delta F508$ CFTR single-channel recording at 35 °C is shown from left to right. Five independent experiments with total recording time of 42 min were used to calculate single-channel parameters $P_o = 0.53 \pm 0.04$ and $\gamma = 13.1 \pm 0.2$ pS. (c) $\Delta RI/\Delta F508$ CFTR single-channel recording during continuous temperature increase from +35 to +40 °C. After 3 min of recording at +35 °C the temperature was increased at a constant rate of 1 °C/min up to +40 °C and kept at this temperature for the last 2 min. The current temperature in the chamber was monitored and shown above the trace. (d) Two minutes of $\Delta RI/\Delta F508$ CFTR single-channel recording at +40 °C is shown on the right. All-points histogram used to calculate P_o and γ is shown at the left. Three independent experiments with total recording time of 21 min were used to calculate single-channel parameters $P_o = 0.65 \pm 0.03$ and $\gamma = 14.1 \pm 0.2$ pS. All data are shown as mean values \pm SEM.

MSD,¹¹ the extent of perturbation elsewhere in the molecule is less evident. Comparison of the X-ray structures of isolated wild-type and $\Delta F508$ NBD1 showed that the overall fold was unaltered.¹² A more recent extensive analysis of structures of multiple wild-type and mutant NBD1s with or without several solubilizing substitutions confirmed that differences were restricted to the small F508-containing surface patch, although several other surface regions appeared to be quite mobile in all of

these structures.³⁷ The same study, using hydrogen/deuterium exchange measurements to address structural dynamics of the domain, essentially confirmed the crystallography findings. Nevertheless, it is known that second-site substitutions of residues at locations quite separate from F508 can compensate for the effects of its deletion.³⁷ These findings indicate that specific structural features of the domain do determine the impact of the mutation.

Although shown not to be essential to CFTR channel function,¹⁶ the RI is a unique feature of NBD1, and in the current study we have determined that it strongly influences the impact of the $\Delta F508$ mutation. First, we confirmed that, in mammalian cells, as in *Xenopus* oocytes, RI is not essential to the biogenesis, stability and function of wild-type CFTR. In fact, the steady-state amount of the RI-deleted protein in transiently transfected HEK cells is greater than that of the wild-type CFTR (Fig. 2a and Fig. S1). While our preliminary single-channel analysis indicates that gating may be somewhat slowed, open probability is not greatly reduced. The effects of RI removal on $\Delta F508$ CFTR were much more pronounced. Maturation was increased to a level at least one third that of the wild type, and

those molecules that did mature were very active with open probability not much less than wild type (Figs. 7 and 8). Even more impressive was the stability of the $\Delta RI/\Delta F508$ protein in terms of both its lifetime in cells and its channel activity at elevated temperature. The rate of turnover of the mutant mature form was not less than that of the wild type (Fig. 3a), and robust channel gating persisted at temperatures up to at least 40 °C (Fig. 7). This increased thermostability of the channel, consistent with that observed with isolated NBD1,¹⁷ is especially notable because it has not been observed with other manipulations to rescue $\Delta F508$ such as growth of cells at reduced temperature or in the presence of known correcting small molecules.

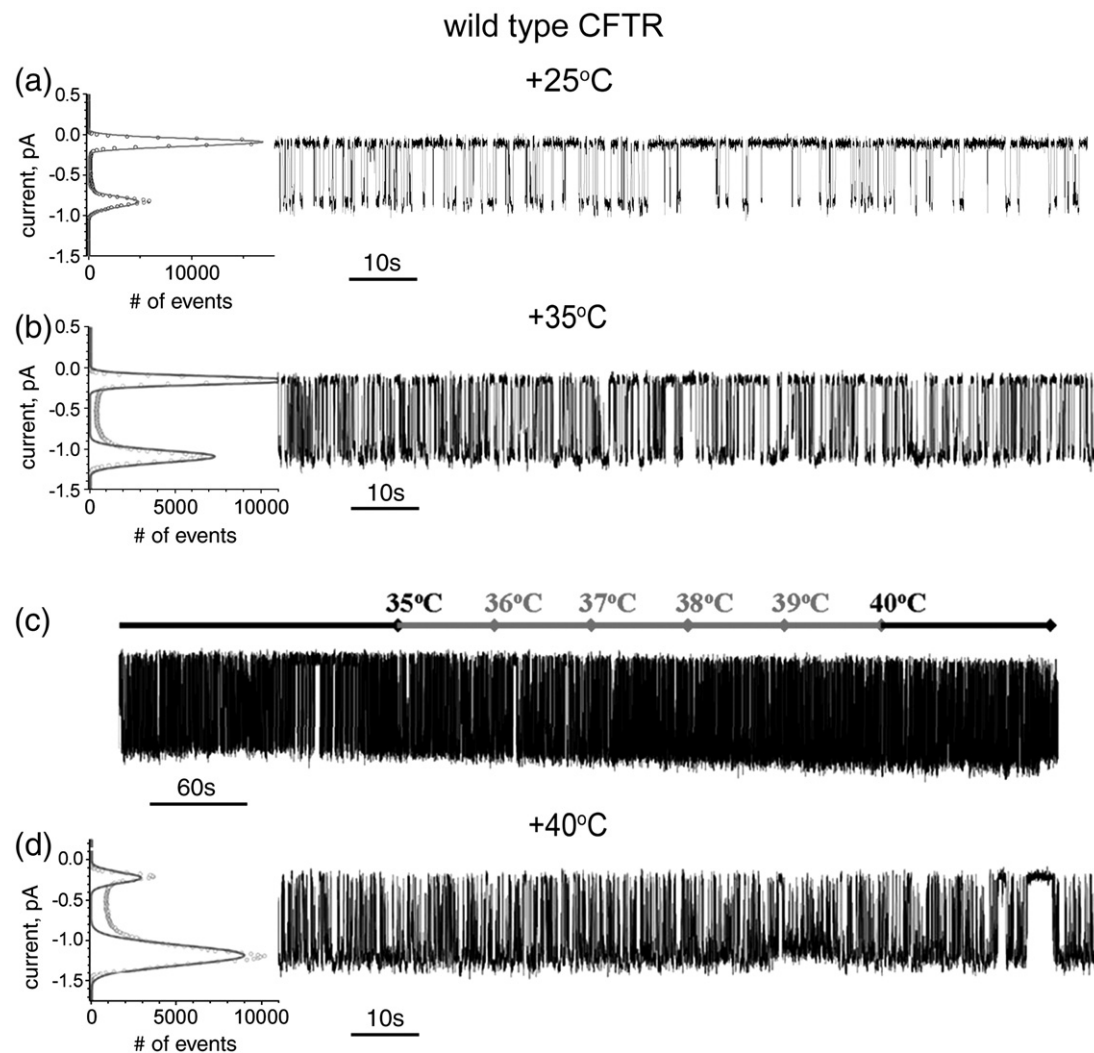


Fig. 8. Influence of temperature on wild-type CFTR gating. (a) All-points histogram and 2 min of wild-type CFTR single-channel recording at 25 °C are shown from left to right. The single-channel parameters $P_o = 0.26 \pm 0.03$ and $\gamma = 10.7 \pm 0.3$ pS were derived from a total recording time of 38 min in four independent experiments. (b) All-points histogram and 2 min of wild-type CFTR single channel recording at 35 °C are shown from left to right. The single channel parameters $P_o = 0.61 \pm 0.04$ and $\gamma = 13.1 \pm 0.3$ pS were calculated from 6 independent experiments with total recording time of 56 min. (c) Temperature ramp. After 3 min of recording at 35 °C the temperature was increased at a constant rate of 1 °C/min up to 40 °C and kept at this temperature for the last 2 min. The current temperature in the chamber is shown above the trace. (d) All-points histogram and 2 min of wild-type CFTR single-channel recording at 40 °C. $P_o = 0.74 \pm 0.05$ and $\gamma = 14.1 \pm 0.3$ pS. A total recording time of 34 min from four independent experiments was used to calculate mean values. Data are shown as mean \pm SEM.

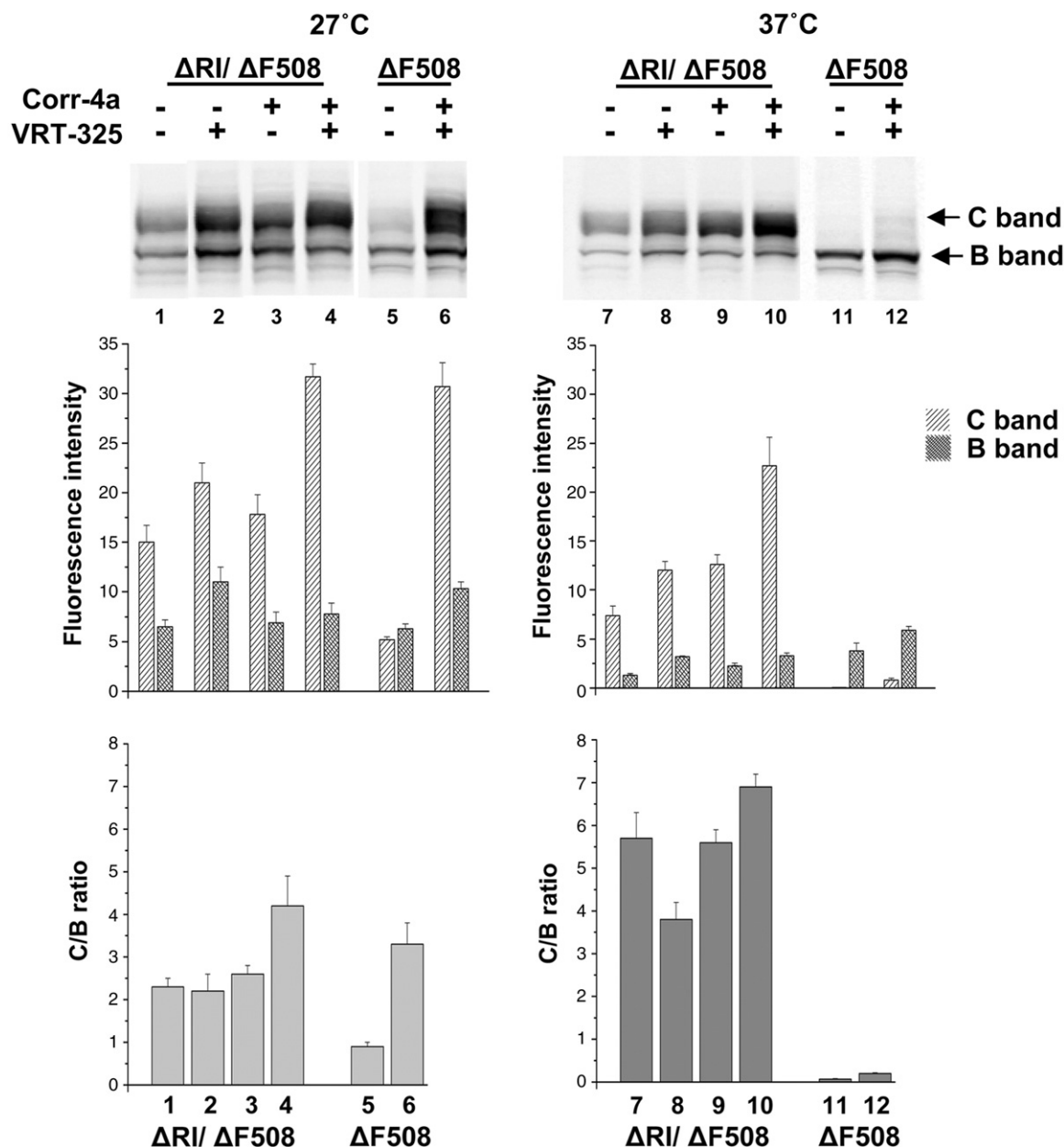


Fig. 9. RI deletion and small-molecule correctors have additive effects on $\Delta F508$ CFTR maturation. $\Delta RI / \Delta F508$ CFTR expressing BHK cells were grown in the presence or absence of 10 μM Corr-4a or VRT-325 or their combination at 27 or 37 $^{\circ}C$ for last the 24 h before harvesting. Whole-cell extracts were then subjected to SDS-PAGE and immunoblot analysis with mAb596. The positions of mature (C) and immature (B) CFTR bands are indicated. The relative fluorescence intensities of these bands as measured at 800 nm in a Li-Cor Odyssey Imager are shown in the bar graphs immediately below the blots and the C band to B band ratios below these.

In addition to stabilization of channel activity, RI deletion also restored the ability of $\Delta F508$ CFTR to bind and occlude ATP at NBD1 up to 35 $^{\circ}C$ (Fig. 4). This effect is consistent with the increased nucleotide-binding affinity of isolated NBD1 from which RI was removed¹⁷ and shows that RI, although located proximal to the bound nucleotide, is not necessary for occlusion.

Our experimental data do not explain how the RI segment of NBD1, far separated from F508 in the structure, has such a strong influence on the mutant protein. However, computational analysis of NBD1

dynamics revealed a dynamic correlation between the F508-containing loop and the F1-like ATP binding core subdomain (Fig. 10), suggesting a coupling between them that is completely absent in the $\Delta F508$ mutant. The ability to restore this coupling in the $\Delta F508$ CFTR upon RI deletion is consistent with the possibility that RI attenuates this process by interaction with the F1-like ATP-binding core subdomain. Because the 507–511 loop is involved in the formation of the NBD1–CL4 interface¹¹ in full-length CFTR (Fig. 10d), RI might indirectly influence the interaction of NBD1 with the

rest of the protein by attenuating the coupling of the 507–511 loop with the F1-like ATP-binding core subdomain of NBD1.

Considering the strong influence of RI on the processing and stability of $\Delta F508$ CFTR together with the likelihood that the peptide may normally assume different conformational states within the complete CFTR molecule,^{36,44} one might postulate that restriction to one of these states would improve maturation of the mutant protein. Conceivably, this might be achieved by the binding of a specific ligand

targeted to the peptide. The possible utility of such reagents in combination with existing partially effective small molecules⁴⁵ that presumably act at other sites is illustrated by the fact that the latter are much more effective when RI is absent (Fig. 9). Combination of an RI restricting agent with existing correctors might be anticipated to have similar additive effects. Related to the idea of combining different modulating agents, it should not be expected that the RI is solely responsible for the sensitivity of CFTR to the $\Delta F508$ mutation because

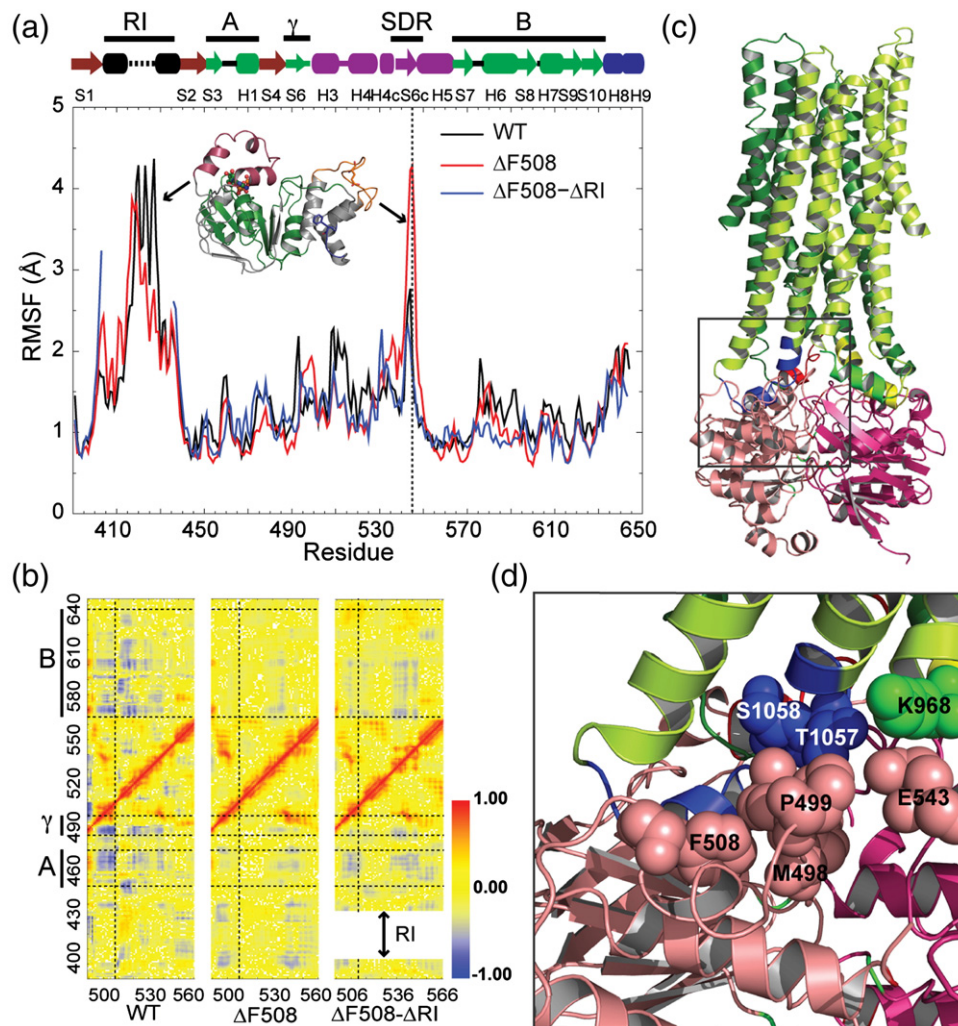


Fig. 10. Dynamics of CFTR NBD1 from DMD simulations. (a) Dynamic flexibility of regions in NBD1 was measured as RMSF. The vertical dotted line indicates fluctuations of the loop containing the E543 site. Structural regions corresponding to the peaks in the plot are shown by arrows. Secondary structural elements of NBD1 are represented by the arrows and cylinders above. The two portions of the F1-ATP-binding core subdomain (A, G451–L475; B, D565–Q637) and γ -switch (Q493–P499) are colored green and labeled by the bold lines at the top for further reference. (b) Pairwise correlation map of the velocities of the C α atoms in the 490–560 region with those of all other segments of NBD1. The regions of the F1-like ATP-binding core subdomain (A and B) and γ -switch are marked by bold lines on the left of the y -axis and continued throughout the graphs as pairs of horizontal dotted lines. The vertical dotted line shows the position of F508. The shift in the x -axis of the $\Delta F508$ – ΔRI correlation map is a consequence of RI deletion. The color code is shown on the right with red (correlation coefficient = 1), indicating residue pairs that move in concert in the same direction, and blue (correlation coefficient = –1), indicating residue pairs that move with opposite velocity all the time. (c) Structural model of full-length CFTR (<http://dokhlab.unc.edu/research/CFTR/home.html>). The area of the NBD1–CL3–CL4 interface is boxed for further detailed consideration in (d). (d) Detailed view of the location and orientation of the residues in the NBD1–CL3–CL4 interface shown inside the box in (c). Residues F508, P499, M498 and E543 from NBD1 (salmon), S1058 and T1057 from CL4 (blue) and K968 from CL3 (cyan) are shown as spheres.

the related ABC transporters, P-glycoprotein and MRP1, lacking RI, also are misprocessed when an aromatic residue in the counterparts of the F508 position is deleted.^{46,47}

We focused primarily on the impact of RI on Δ F508 CFTR rather than the wild type because of the potential practical significance of being able to positively impact the mutant. However, the functional role of RI in the wild-type protein still seems somewhat enigmatic, since despite its presence in all species where CFTR is expressed, it is not essential to chloride channel activity.¹⁶ More extensive studies are required to reveal the advantage of RI to wild-type CFTR function. As yet we have not definitively determined whether the wild-type CFTR channel's thermostability is further increased when RI is not present.

In summary, while the exact functional role of the unique RI in NBD1 of wild-type CFTR remains to be elucidated, we have found that it is a major contributor to the instability and dysfunction of Δ F508 CFTR responsible for most cystic fibrosis and as such may be a target for therapeutic agents that would diminish these effects.

Materials and Methods

Materials

Mouse monoclonal CFTR antibodies to epitopes in the N-terminus [monoclonal antibody (mAb) 13-4], R domain (mAb570) and NBD2 (mAb596) were generated as described.⁴⁸ Goat anti-mouse IgG-IR800 was from LiCor Corp. (Lincoln, NE), and goat anti-mouse IgG-AlexaFluor 488 was from Invitrogen (Carlsbad, CA). Small-molecule correctors VRT-325 and Corr-4a were generously provided by the Cystic Fibrosis Foundation.

CFTR construction and expression

The Δ RI/ Δ F508 CFTR comprises human wild-type CFTR protein with residues 404–435 and 508 deleted. Human CFTR cDNAs encoding wild-type or mutant proteins were expressed transiently in HEK 293 cells, or stably in BHK-21 cells, with pcDNA3 and pNUT vectors, respectively, as described previously.²⁶ Δ RI/ Δ F508 CFTR constructs in pcDNA3 and pNUT vectors were generated from human wild-type CFTR cDNA using the Quick Exchange protocol (Stratagene) as described, and sequences were confirmed by automated DNA sequencing (UNC-CH Genome Analysis Facility). Transfection was carried out using jetPEI transfection reagent (Fermentas, Glen Burnie, MD) according to the manufacturer's instructions. For stable cell line establishment, BHK cells expressing CFTR were selected and maintained in methotrexate-containing media as previously described.⁴⁹

Western blot and immunofluorescence microscopy

HEK or BHK cells overexpressing CFTR were harvested in radioimmunoprecipitation assay (RIPA) buffer without SDS (50 mM Tris, 150 mM NaCl, 1% Triton X-100, 1% deoxycholate, pH 7.4) plus protease inhibitor cocktail

(1 μ g/ml leupeptin, 2 μ g/ml aprotinin, 3.57 μ g/ml E64, 156.6 μ g/ml benzamidin and 2 mM Pefablock) and equal amounts of proteins in SDS-PAGE sample buffer were subjected to 7.5% SDS-PAGE and Western blot analysis with mAb596 to determine CFTR expression and maturation.²⁴

To determine the subcellular distribution of CFTR, BHK-21 cells grown in glass-bottom culture dishes (MatTek Corporation) were fixed with 4% paraformaldehyde, permeabilized with 0.1% saponin, and blocked with 1% bovine serum albumin and 5% normal goat serum. CFTR localization was detected by mAb570 in combination with Alexa Fluor 488-conjugated goat-anti-mouse IgG using a Zeiss LSM510 confocal laser scanning microscope.

Metabolic pulse-chase labeling

BHK cells stably expressing wild-type and mutant CFTR were pulsed labeled with [³⁵S]methionine and chased as previously described.⁵⁰ Briefly, BHK cells expressing wild-type protein or Δ F508/ Δ RI were grown to 80% confluency in 60-mm dishes. Cells were then labeled with 100 μ Ci per plate [³⁵S]methionine (Perkin Elmer, >1000 Ci/mmol) for 8 h in a cocktail of 90% methionine-free medium, 10% normal growth medium and 10% fetal bovine serum. After labeling, cells were washed two times with phosphate-buffered saline and chased using growth medium supplemented with 1 mM cold methionine. At the end of the chase period, cells were washed twice with phosphate-buffered saline and solubilized with 1 ml of RIPA buffer containing protease inhibitors. CFTR was immunoprecipitated using antibody 596 and Protein A beads (Invitrogen). Gels were fixed in 10% acetic acid/30% methanol, washed in water, then soaked in 1 M sodium salicylate and dried onto filter paper for fluorography. Electronic autoradiography was performed on the dried gels using a Packard Instant Imager.

Iodide efflux assay

BHK cells stably expressing wild-type and mutant CFTR grown to ~100% confluence in six-well plates were incubated in an iodide loading buffer (136 mM NaI, 3 mM KNO₃, 2 mM Ca(NO₃)₂, 11 mM glucose and 20 mM Hepes, pH 7.4) for 1 h at room temperature. Extracellular iodide was removed by rinsing the cells with iodide-free efflux buffer (same as the loading buffer except NaNO₃ replaced NaI). Samples were collected by completely replacing the efflux buffer (1 ml volume) with fresh solution at 1-min intervals. The first four samples were used to establish the baseline. An iodide efflux upon stimulation with PKA agonists (10 μ M forskolin, 100 μ M dibutyl-cAMP and 1 mM 3-isobutyl-1-methylxanthine) were measured using an iodide-selective electrode LIS-146ICM (Lazar Res. Lab., Inc.), as previously described.⁴⁹

Membrane isolation

BHK or HEK 293 cells expressing CFTR variants were harvested by scraping, and then homogenized on ice in 10 mM Hepes, pH 7.2, 1 mM EDTA (ethylenediaminetetraacetic acid) containing a protease inhibitor cocktail (benzamidin at 120 μ g/ml, E64 at 3.5 μ g/ml, aprotinin at 2 μ g/ml, leupeptin at 1 μ g/ml and Pefabloc at 50 μ g/ml). Centrifugation at 600g for 15 min removed nuclei and undisturbed cells. The supernatant was centrifuged at

100,000g for 60 min to pellet membranes, which were then resuspended in phosphorylation buffer [10 mM Hepes, pH 7.2, containing 0.5 mM EGTA (ethylene glycol bis(β -aminoethyl ether) N,N' -tetraacetic acid), 2 mM $MgCl_2$, and 250 mM sucrose]. Brief (3×20 s) bath sonication was used to generate vesicles of uniform size. For the single-channel recordings, membrane vesicles were phosphorylated by incubation with 50 nM PKA catalytic subunit (Promega) and 2 mM Na_2ATP (Sigma) in phosphorylation buffer for 20 min at $+4^\circ C$. The membranes were aliquoted and stored at $-80^\circ C$ until used.

Photoaffinity labeling

CFTR nucleotide binding and retention assays were performed essentially as described previously.⁵¹ Briefly, membrane suspensions were incubated either at 4 or $35^\circ C$ for 5 min with 25 μM [γ - ^{32}P] N_3ATP . The labeled membranes were then UV-irradiated directly (Stratalinker UV cross-linker) or after pelleting and washing away unbound nucleotide. To monitor the [γ - ^{32}P] N_3ATP dissociation from the nucleotide-binding site, the washed membranes were resuspended in nucleotide-free buffer and UV-irradiated after incubation at $35^\circ C$ for various periods of time. After limited trypsin digestion for 15 min on ice, the labeled membranes were solubilized in RIPA buffer, and CFTR fragments were immunoprecipitated with mAb13-4 or mAb596. The immunoprecipitates were fractionated by SDS-PAGE (4–20% acrylamide) and transferred onto nitrocellulose membranes for autoradiography [X-ray films and Packard Instant Imager (PerkinElmer)] for quantification of ^{32}P radioactivity associated with NBD1- and NBD2-containing bands.

Single-channel measurements

Planar lipid bilayers were prepared by painting a 0.2 mm hole drilled in a Teflon cup with a phospholipids solution in *n*-decane containing a 3:1 mixture of 1-palmitoyl-2-oleoyl-*sn*-glycero-3-phosphoethanolamine and 1-palmitoyl-2-oleoyl-*sn*-glycero-3-phosphoserine (Avanti Polar Lipids). The lipid bilayer separated 1.0 ml of solution in the Teflon cup (cis side) from 5.0 ml of a solution in an outer glass chamber (trans side). Both chambers were magnetically stirred and thermally insulated. Heating and temperature control were established by a temperature control system (TC2BIP, Cell Micro Controls).

CFTR ion channels were transferred into the preformed lipid bilayer by spontaneous fusion of membrane vesicles containing CFTR variants. To maintain uniform orientation and functional activity of CFTR channels transferred into the bilayer, 2 mM ATP, 50 nM PKA and membrane vesicles were added in the cis compartment only. All measurements were done in symmetrical salt solution (300 mM Tris-HCl, pH 7.2, 3 mM $MgCl_2$ and 1 mM EGTA) under voltage-clamp conditions by using an Axopatch 200B amplifier. The membrane voltage potential of -75 mV is the difference between cis and trans (ground) compartments. The data analysis was performed as described before.⁵²

DMD simulations

Equilibrium DMD simulations^{34,35} of wild-type, $\Delta F508$ and $\Delta F508$ - ΔRI CFTR NBD1 were performed for 10^5 DMD time units (approximately 5 ns). The initial

coordinates were obtained from the crystal structure of NBD1 [Protein Data Bank (PDB) codes 2BBO and 2BBT], and the system was pre-relaxed before performing long simulations. To obtain the dynamic coupling pattern of structurally distant regions, we performed free simulations without holding any part of the protein fixed during the simulations. The dynamic coupling of different constructs of NBD1 was obtained by computing normalized correlation matrices^{53,54} from DMD simulation trajectories. In the calculation of RMSF of each residue in NBD1 over the course of the simulation, the translational and rotational freedom were reduced by translating the center of mass of the protein to the origin before aligning each snapshot with respect to the average structure.

Statistical analysis

Results are presented as mean \pm SEM. Statistical significances were calculated by using Student's *t* test. *P* values of less than 0.05 were considered significant.

Acknowledgements

This work was supported by grants from the NIH to J.R.R. (DK051870) and N.V.D. (GM080742) and from the Cystic Fibrosis Foundation. We thank Dr. Adrian W. R. Serohijos for useful discussions and preliminary DMD simulations of RI impact on NBD1 dynamics.

Supplementary Data

Supplementary data associated with this article can be found, in the online version, at [doi:10.1016/j.jmb.2010.06.019](https://doi.org/10.1016/j.jmb.2010.06.019)

References

1. Aleksandrov, A. A., Aleksandrov, L. A. & Riordan, J. R. (2007). CFTR (ABCC7) is a hydrolyzable-ligand-gated channel. *Pflugers Arch.* **453**, 693–702.
2. Wang, W., Wu, J., Bernard, K., Li, G., Wang, G., Bevensee, M. O. & Kirk, K. L. (2010). ATP-independent CFTR channel gating and allosteric modulation by phosphorylation. *Proc. Natl Acad. Sci. USA*, **107**, 3888–3893.
3. Riordan, J. R. (2008). CFTR function and prospects for therapy. *Annu. Rev. Biochem.* **77**, 701–726.
4. Denning, G. M., Anderson, M. P., Amara, J. F., Marshall, J., Smith, A. E. & Welsh, M. J. (1992). Processing of mutant cystic fibrosis transmembrane conductance regulator is temperature-sensitive. *Nature*, **358**, 761–764.
5. Howard, M., Fischer, H., Roux, J., Santos, B. C., Gullans, S. R., Yancey, P. H. & Welch, W. J. (2003). Mammalian osmolytes and S-nitrosoglutathione promote Delta F508 cystic fibrosis transmembrane conductance regulator (CFTR) protein maturation and function. *J. Biol. Chem.* **278**, 35159–35167.
6. Wang, X., Koulov, A. V., Kellner, W. A., Riordan, J. R. & Balch, W. E. (2008). Chemical and biological folding

- contribute to temperature-sensitive DeltaF508 CFTR trafficking. *Traffic*, **9**, 1878–1893.
7. Pedemonte, N., Lukacs, G. L., Du, K., Caci, E., Zegarar-Moran, O., Galletta, L. J. & Verkman, A. S. (2005). Small-molecule correctors of defective DeltaF508-CFTR cellular processing identified by high-throughput screening. *J. Clin. Invest.* **115**, 2564–2571.
 8. Pissarra, L. S., Farinha, C. M., Xu, Z., Schmidt, A., Thibodeau, P. H., Cai, Z. *et al.* (2008). Solubilizing mutations used to crystallize one CFTR domain attenuate the trafficking and channel defects caused by the major cystic fibrosis mutation. *Chem. Biol.* **15**, 62–69.
 9. Teem, J. L., Berger, H. A., Ostedgaard, L. S., Rich, D. P., Tsui, L. C. & Welsh, M. J. (1993). Identification of revertants for the cystic fibrosis $\Delta F508$ mutation using STE6-CFTR chimeras in yeast. *Cell*, **73**, 335–346.
 10. DeCarvalho, A. C., Gansheroff, L. J. & Teem, J. L. (2002). Mutations in the nucleotide binding domain 1 signature motif region rescue processing and functional defects of cystic fibrosis transmembrane conductance regulator Delta F508. *J. Biol. Chem.* **277**, 35896–35905.
 11. Serohijos, A. W., Hegedus, T., Aleksandrov, A. A., He, L., Cui, L., Dokholyan, N. V. & Riordan, J. R. (2008). Phenylalanine-508 mediates a cytoplasmic-membrane domain contact in the CFTR 3D structure crucial to assembly and channel function. *Proc. Natl Acad. Sci. USA*, **105**, 3256–3261.
 12. Lewis, H. A., Zhao, X., Wang, C., Sauder, J. M., Rooney, I., Noland, B. W. *et al.* (2005). Impact of the DeltaF508 mutation in first nucleotide-binding domain of human cystic fibrosis transmembrane conductance regulator on domain folding and structure. *J. Biol. Chem.* **280**, 1346–1353.
 13. Qu, B. H., Strickland, E. H. & Thomas, P. J. (1997). Localization and suppression of a kinetic defect in cystic fibrosis transmembrane conductance regulator folding. *J. Biol. Chem.* **272**, 15739–15744.
 14. Serohijos, A. W., Hegedus, T., Riordan, J. R. & Dokholyan, N. V. (2008). Diminished self-chaperoning activity of the DeltaF508 mutant of CFTR results in protein misfolding. *PLoS Comput. Biol.* **4**, e1000008.
 15. Lewis, H. A., Buchanan, S. G., Burley, S. K., Connors, K., Dickey, M., Dorwart, M. *et al.* (2004). Structure of nucleotide-binding domain 1 of the cystic fibrosis transmembrane conductance regulator. *EMBO J.* **23**, 282–293.
 16. Csanady, L., Chan, K. W., Nairn, A. C. & Gadsby, D. C. (2005). Functional roles of nonconserved structural segments in CFTR's NH₂-terminal nucleotide binding domain. *J. Gen. Physiol.* **125**, 43–55.
 17. Atwell, S., Brouillette, C. G., Connors, K., Emtage, S., Gheyi, T., Guggino, W. *et al.* (2010). Structures of a minimal human CFTR first nucleotide-binding domain as a monomer, head-to-tail homodimer, and pathogenic mutant. *Protein Eng. Des. Sel.* **23**, 375–384.
 18. Yang, H., Shelat, A. A., Guy, R. K., Gopinath, V. S., Ma, T., Du, K. *et al.* (2003). Nanomolar affinity small molecule correctors of defective Delta F508-CFTR chloride channel gating. *J. Biol. Chem.* **278**, 35079–35085.
 19. Sharma, M., Pampinella, F., Nemes, C., Benharouga, M., So, J., Du, K. *et al.* (2004). Misfolding diverts CFTR from recycling to degradation: quality control at early endosomes. *J. Cell. Biol.* **164**, 923–933.
 20. Glozman, R., Okiyoneda, T., Mulvihill, C. M., Rini, J. M., Barriere, H. & Lukacs, G. L. (2009). N-Glycans are direct determinants of CFTR folding and stability in secretory and endocytic membrane traffic. *J. Cell. Biol.* **184**, 847–862.
 21. Du, K., Sharma, M. & Lukacs, G. L. (2005). The DeltaF508 cystic fibrosis mutation impairs domain-domain interactions and arrests post-translational folding of CFTR. *Nat. Struct. Mol. Biol.* **12**, 17–25.
 22. Aleksandrov, L., Aleksandrov, A. A., Chang, X. B. & Riordan, J. R. (2002). The first nucleotide binding domain of cystic fibrosis transmembrane conductance regulator is a site of stable nucleotide interaction, whereas the second is a site of rapid turnover. *J. Biol. Chem.* **277**, 15419–15425.
 23. Basso, C., Vergani, P., Nairn, A. C. & Gadsby, D. C. (2003). Prolonged nonhydrolytic interaction of nucleotide with CFTR's NH₂-terminal nucleotide binding domain and its role in channel gating. *J. Gen. Physiol.* **122**, 333–348.
 24. Cui, L., Aleksandrov, L., Hou, Y. X., Gentzsch, M., Chen, J. H., Riordan, J. R. & Aleksandrov, A. A. (2006). The role of cystic fibrosis transmembrane conductance regulator phenylalanine 508 side chain in ion channel gating. *J. Physiol.* **572**, 347–358.
 25. Aleksandrov, L., Aleksandrov, A. & Riordan, J. R. (2008). Mg²⁺-dependent ATP occlusion at the first nucleotide-binding domain (NBD1) of CFTR does not require the second (NBD2). *Biochem. J.* **416**, 129–136.
 26. He, L., Aleksandrov, A. A., Serohijos, A. W., Hegedus, T., Aleksandrov, L. A., Cui, L. *et al.* (2008). Multiple membrane-cytoplasmic domain contacts in the cystic fibrosis transmembrane conductance regulator (CFTR) mediate regulation of channel gating. *J. Biol. Chem.* **283**, 26383–26390.
 27. Dalemans, W., Barbry, P., Champigny, G., Jallat, S., Dott, K., Dreyer, D. *et al.* (1991). Altered chloride-ion channel kinetics associated with the Delta-F508 cystic-fibrosis mutation. *Nature*, **354**, 526–528.
 28. Haws, C. M., Nepomuceno, I. B., Krouse, M. E., Wakelee, H., Law, T., Xia, Y. *et al.* (1996). DeltaF508-CFTR channels: kinetics, activation by forskolin, and potentiation by xanthines. *Am. J. Physiol.* **270**, C1544–C1555.
 29. Schultz, B. D., Frizzell, R. A. & Bridges, R. J. (1999). Rescue of dysfunctional DeltaF508-CFTR chloride channel activity by IBMX. *J. Membr. Biol.* **170**, 51–66.
 30. Wang, F., Zeltwanger, S., Hu, S. & Hwang, T. C. (2000). Deletion of phenylalanine 508 causes attenuated phosphorylation-dependent activation of CFTR chloride channels. *J. Physiol.* **524**(Pt 3), 637–648.
 31. Hegedus, T., Aleksandrov, A., Cui, L., Gentzsch, M., Chang, X. B. & Riordan, J. R. (2006). F508del CFTR with two altered RXR motifs escapes from ER quality control but its channel activity is thermally sensitive. *Biochim. Biophys. Acta*, **1758**, 565–572.
 32. Jurkuvenaite, A., Chen, L., Bartoszewski, R., Goldstein, R., Bebok, Z., Matalon, S. & Collawn, J. F. (2010). Functional stability of rescued Delta F508 cystic fibrosis transmembrane conductance regulator in airway epithelial cells. *Am. J. Respir. Cell Mol. Biol.* **42**, 363–372.
 33. Van Goor, F., Straley, K. S., Cao, D., Gonzalez, J., Hadida, S., Hazlewood, A. *et al.* (2006). Rescue of DeltaF508-CFTR trafficking and gating in human cystic fibrosis airway primary cultures by small molecules. *Am. J. Physiol. Lung Cell Mol. Physiol.* **290**, L1117–L1130.
 34. Dokholyan, N. V., Buldyrev, S. V., Stanley, H. E. & Shakhnovich, E. I. (1998). Discrete molecular dynamics studies of the folding of a protein-like model. *Fold. Des.* **3**, 577–587.

35. Ding, F. & Dokholyan, N. V. (2006). Emergence of protein fold families through rational design. *PLoS Comput. Biol.* **e85**, 2.
36. Kanelis, V., Hudson, R. P., Thibodeau, P. H., Thomas, P. J. & Forman-Kay, J. D. (2010). NMR evidence for differential phosphorylation-dependent interactions in WT and $\Delta F508$ CFTR. *EMBO J.* **29**, 263–277.
37. Lewis, H. A., Wang, C., Zhao, X., Hamuro, Y., Connors, K., Kearins, M. C. *et al.* (2010). Structure and dynamics of NBD1 from CFTR characterized using crystallography and hydrogen/deuterium exchange mass spectrometry. *J. Mol. Biol.* **396**, 406–430.
38. Schmitt, L., Benabdelhak, H., Blight, M. A., Holland, I. B. & Stubbs, M. T. (2003). Crystal structure of the nucleotide-binding domain of the ABC-transporter haemolysin B: identification of a variable region within ABC helical domains. *J. Mol. Biol.* **330**, 333–342.
39. Ward, C. L., Omura, S. & Kopito, R. R. (1995). Degradation of CFTR by the ubiquitin-proteasome pathway. *Cell*, **83**, 121–127.
40. Jensen, T. J., Loo, M. A., Pind, S., Williams, D. B., Goldberg, A. L. & Riordan, J. R. (1995). Multiple proteolytic systems, including the proteasome, contribute to CFTR processing. *Cell*, **83**, 129–135.
41. Grove, D. E., Rosser, M. F., Ren, H. Y., Naren, A. P. & Cyr, D. M. (2009). Mechanisms for rescue of correctable folding defects in CFTR $\Delta F508$. *Mol. Biol. Cell*, **20**, 4059–4069.
42. Wang, X., Venable, J., LaPointe, P., Hutt, D. M., Koulov, A. V., Coppinger, J. *et al.* (2006). Hsp90 cochaperone Aha1 downregulation rescues misfolding of CFTR in cystic fibrosis. *Cell*, **127**, 803–815.
43. Wang, Y., Loo, T. W., Bartlett, M. C. & Clarke, D. M. (2007). Correctors promote maturation of cystic fibrosis transmembrane conductance regulator (CFTR)-processing mutants by binding to the protein. *J. Biol. Chem.* **282**, 33247–33251.
44. Mornon, J. P., Lehn, P. & Callebaut, I. (2009). Molecular models of the open and closed states of the whole human CFTR protein. *Cell. Mol. Life Sci.* **66**, 3469–3486.
45. Wang, Y., Loo, T. W., Bartlett, M. C. & Clarke, D. M. (2007). Additive effect of multiple pharmacological chaperones on maturation of CFTR processing mutants. *Biochem. J.* **406**, 257–263.
46. Loo, T. W., Bartlett, M. C. & Clarke, D. M. (2002). Introduction of the most common cystic fibrosis mutation ($\Delta F508$) into human P-glycoprotein disrupts packing of the transmembrane segments. *J. Biol. Chem.* **277**, 27585–27588.
47. Buyse, F., Vandenbranden, M. & Ruyschaert, J. M. (2004). Mistargeted MRP $\Delta F728$ mutant is rescued by intracellular GSH. *FEBS Lett.* **578**, 145–151.
48. Cui, L., Aleksandrov, L., Chang, X. B., Hou, Y. X., He, L., Hegedus, T. *et al.* (2007). Domain interdependence in the biosynthetic assembly of CFTR. *J. Mol. Biol.* **365**, 981–994.
49. Chang, X. B., Tabcharani, J. A., Hou, Y. X., Jensen, T. J., Kartner, N., Alon, N. *et al.* (1993). Protein kinase A (PKA) still activates CFTR chloride channel after mutagenesis of all ten PKA consensus phosphorylation sites. *J. Biol. Chem.* **268**, 11304–11311.
50. Loo, M. A., Jensen, T. J., Cui, L., Hou, Y., Chang, X. B. & Riordan, J. R. (1998). Perturbation of Hsp90 interaction with nascent CFTR prevents its maturation and accelerates its degradation by the proteasome. *EMBO J.* **17**, 6879–6887.
51. Aleksandrov, L., Mengos, A., Chang, X., Aleksandrov, A. & Riordan, J. R. (2001). Differential interactions of nucleotides at the two nucleotide binding domains of the cystic fibrosis transmembrane conductance regulator. *J. Biol. Chem.* **276**, 12918–12923.
52. Aleksandrov, A. A., Cui, L. & Riordan, J. R. (2009). Relationship between nucleotide binding and ion channel gating in cystic fibrosis transmembrane conductance regulator. *J. Physiol.* **587**, 2875–2886.
53. Sharma, S., Ding, F. & Dokholyan, N. V. (2007). Multiscale modeling of nucleosome dynamics. *Biophys. J.* **92**, 1457–1470.
54. Teotico, D. G., Frazier, M. L., Ding, F., Dokholyan, N. V., Temple, B. R. & Redinbo, M. R. (2008). Active nuclear receptors exhibit highly correlated AF-2 domain motions. *PLoS Comput. Biol.* **4**, e1000111.